scientific reports

OPEN

Coupling between topological edge state and defect mode-based biosensor using phononic crystal

Zaky A. Zaky[1,2,3]✉, M. Al-Dossari[4], Ahmed S. Hendy[5], Yassine Bouazzi[6], Attia Boudjemline[6] & Arafa H. Aly[1]

A wealth of details regarding an individual's state of health, like a person's respiratory and metabolic functioning, can be studied by analyzing the volatile molecules and atoms in human exhaled breath. Besides, the salinity of seawater is a crucial factor in understanding its characteristics because any variation in the salinity of seawater represents the variations in the hydrological, biological, and chemical distributions. In this paper, a symmetrical one-dimensional phononic structure is theoretically designed using two symmetrical crystals separated with a defective cavity. This structure has been designed to excite a topological edge state coupled with defect mode. The coupled mode achieves high sensitivity to NaCl concentration in an aqueous solution, seven times higher than the defective one. By ranging the NaCl concentration from 0 to 21%, the average sensitivity is 467 and 3160 Hz/% for defect mode and coupled modes, respectively. The bandwidth of the coupled mode of 170 Hz is much narrower than that of the defect mode of 671 Hz for detecting salinity. For detecting the increase in CO_2 concentration in dry exhaled breath by ranging the CO_2 concentration from 0 ppm to 100 ppm, the average sensitivity is 32 Hz/ppm for coupled mode. As a result of these enhancements in the sensitivity and bandwidth of the coupled mode, the coupled mode is recommended to be used in different biosensing applications.

Keywords Biosensor, Phononic crystal, Symmetric structures, Bandgap, Topological edge state

Phononic crystals (PnCs) are synthetic materials that are formed periodically, varying their elasticity and mass acoustic properties. PnCs can direct, control, and manipulate phonons or sound waves in liquids, gases, and solids. Phononic band gap (PnBG), acoustic resonator (AR)[1,2], wireless devices[3], and hypersonic PnCs are some of the fundamental properties and applications of PnCs. PnBG stops the propagation of phonons in specific frequency bands. ARs are designed to trap and amplify sound waves at specific frequencies, and PnCs can act as acoustic resonators. However, unresolved issues include the creation of topological phononics and producing sturdy, large-area samples[3].

The periodic structure of one-dimensional PnCs (1D-PnCs), composed of alternating layers of various materials with various elastic properties, provides these materials with distinct acoustic characteristics. These crystals can be used in several industries, including soundproofing, sensing[4,5], and acoustic manipulation. By separating two 1D-PnCs with a defect cavity, acoustic waves with specific energies are localized in this cavity. Alrowaili et al.[6] designed a defective 1D-PnC sensor to detect pollution in water, such as heavy metals of cadmium chloride. As a result of the changes in the acoustic properties owing to the change in the concentration of the analyte, a shift in the AR occurs with a sensitivity (S) of 1904.25 Hz/ppm.

Topological edge states (TESs) are states of matter at a material's boundary when external factors affect the material's attributes[7]. TES in PnCs has been found in a variety of materials and configurations, including graphene-like PnCs[8], hexagonal PnCs[9], and space-time PnCs[10]. Potential uses for TES include communication and manipulation of elastic waves[9]. There is still much to learn about topological edge states in phononic crystals, and there may be opportunities for advancements in materials science and acoustics. Sensors employ TES in various ways, taking advantage of their unique qualities to improve the sensing performance. Several

[1]TH-PPM Group, Physics Department, Faculty of Science, Beni-Suef University, Beni-Suef 62521, Egypt. [2]Academy of Scientific Research and Technology (ASRT), Cairo, Egypt. [3]Frank Laboratory of Neutron Physics, Joint Institute for Nuclear Research, 141980 Dubna, Russia. [4]Dahran Aljanoub Applied College, King Khalid University, Abha 62529, Saudi Arabia. [5]Department of Computational Mathematics and Computer Science, Institute of Natural Sciences and Mathematics, Ural Federal University, 19 Mira St, Yekaterinburg 620002, Russia. [6]Department of Industrial Engineering, College of Engineering, University of Ha'il, Ha'il City 81451, Saudi Arabia. ✉email: zaky.a.zaky@science.bsu.edu.eg

applications and discoveries pertaining to the utilization of TES in sensors have been reported, such as enhanced sensitivity[8], scanning qubit probes[11], photonic sensors[12], and experimental realization[13]. These results imply that TES is promising for improving sensor performance and sensitivity, especially for phononic and photonic sensing applications. These TESs have unique qualities that make them attractive for the creation of next-generation sensor systems, such as resilience to disturbances. Zaky et al.[14] investigated a ternary 1D-PnC of alternative cross-section tubes as a sensor for hazardous gases depending on the TES. Their model has figure of merit (FoM) of 33.7 $\mathrm{m}^{-1}.s$ and S of 1.58 $\mathrm{Hz.m}^{-1}.s$.

The salinity of seawater is a crucial factor in understanding its characteristics[15]. Any variation in this salinity of seawater represents the variations in the hydrological, biological, and chemical distributions. Therefore, the salinity of seawater must be precisely measured onsite. Zhao et al.[16] suggested a fiber grating with a long period to detect salinity in seawater with a sensitivity of 0.889 $\mathrm{nm/m}^{-1}$. Zaky and Arafa designed a 1D-photonic crystal (1D-PC) to detect the temperature and salinity depending on the Tamm resonance[17]. Almawgani et al.[18]. proposed 1D-PC NaCl concentrations in aqueous solution with S of 24700 nm/RIU.

A person's respiratory and metabolic processes can be inferred non-invasively by measuring the exceed of the ratio of CO_2 in Dry exhaled breath (DEB)[19]. Bhagya et al.[20] discussed a detector to monitor CO_2 ratio in DEB to identify different diseases such as chronic obstructive pulmonary. Oort et al.[21] discussed a vital method to analyze the DEB to monitor pneumonia detection. Mazzone et al.[22] investigated the identification of volatile organic compounds in DEB as a biomarker for lung cancer. Zarifi et al.[23] presented a CO_2 microwave sensor. Fayaz et al.[24] designed a high resolution, non-contact sensor using microwave resonator for detecting the exhaustion degree of samples of beaded activated carbon used in a volatile organic compounds abatement system.

This paper theoretically presents a multifunctional sensor based on TES using a 1D-PnC. The optimum acoustic and geometrical parameters are selected based on performance, linearity, full width at half maximum ($FWHM$), and sensitivity. Moreover, the present results, which depend on the coupling between TES and defect mode resonance (DM), will be compared with a similar study that depends only on defect mode resonance[25]. Although Taha et al.[25] designed a similar structure of a periodic symmetric 1D-PnCs separated by a defect cavity, they focused only on DM. They ignored the coupling between the DM and TES. However, the authors' analysis of the density and acoustic speed of salinity water relies on an equation from Ref[17]. and experimental data from Ref[18]. , respectively; the authors didn't adhere to the conditions of these data. Despite the acoustic speed of salinity water is only accurate for salinities up to 21%, as mentioned in Ref[26]. , and the experimental data extended only up to about 26%[27], Taha et al.[25] expanded their study up to NaCl concentration of 60%. Also, they did not explain the shift of peaks to lower frequencies with increasing the concentration of NaCl (with increasing speed); however, the peak was shifted to higher frequencies in other studies[28,29]. In addition, they claimed that the normalized frequency is $\omega\, a/2\pi\, c$, where c is the speed in epoxy, a is the length of the unit cell, and ω is the angular frequency, but their results clear that the normalized frequency in their study is multiplied by a factor of about 2.18 (they mentioned that normalized frequency of 0.991893 equals 0.76706 MHz that coincides with our calculations). Besides, the authors claimed that the peak of pure water (0% NaCl) for low concentrations study is at a frequency of 0.76706 MHz. But, for high-concentration studies, the peak of pure water (0% NaCl) is at a frequency of 1.698439 MHz without any apparent reason. As a result, we decided to discuss these points in this paper. Besides, by testing the CO_2 ratio in DEB, the suggested sensor has high-quality performance.

Materials and methods

The 3D configuration of the proposed detector is presented in Fig. 1. The construction is a periodic symmetrical 1D-PnCs (PnC1 and PnC2) separated by a defect cavity (D). PnC1 and PnC2 are Lead (Pb)/Epoxy and Epoxy*Pb, respectively. N and S represent the unit cell numbers of PnC1 and PnC2, respectively. A, B, and D are layers of Pb, Epoxy, and cavity layer of width d_1, d_2, and d_D. The ambient medium to the sensor is water. The density (ρ_i) and longitudinal velocity (c_i) of Pb, Epoxy, and water are listed in Table 1[25]. Pb and Epoxy can be fabricated cheaply[30,31]. Layer D will be injected with NaCl aqueous solution at room temperature. The cavity layer is surrounded by epoxy layer. Epoxy can resists corrosion for a long time when immersed in a saline solution[32,33].

Transfer matrix method (TMM) is a powerful analytical methodology employed in various fields, such as acoustics, optics, quantum mechanics, and statistical mechanics, to simulate the propagation of acoustic waves[34–36]. TMM is used to study an array of film dispersions in optics and acoustics, which is very important for designing mirrors, sensors, and other devices. The TMM disassembles the structure into a series of elements and computes the transfer matrix by multiplying the matrices. Reflectance and transmittance are obtained from the total matrix of the system.

Assume a normal acoustic wave is incident on the suggested $(\mathrm{PnC1})^N D\, (\mathrm{PnC2})^S$ structure. Each layer can be simulated using the following matrix (m_i)[37,38]:

$$m_i = \begin{bmatrix} m_{11} & m_{12} \\ m_{21} & m_{22} \end{bmatrix},\ i = 1,\ 2,\ and\ D, \tag{1}$$

where,

$$m_{11} = cos\,(k_i d_i)\,, \tag{2}$$

$$m_{12} = -iZ_i sin\,(k_i d_i)\,, \tag{3}$$

$$m_{21} = -i\frac{1}{Z_i} sin\,(k_i d_i)\,, \tag{4}$$

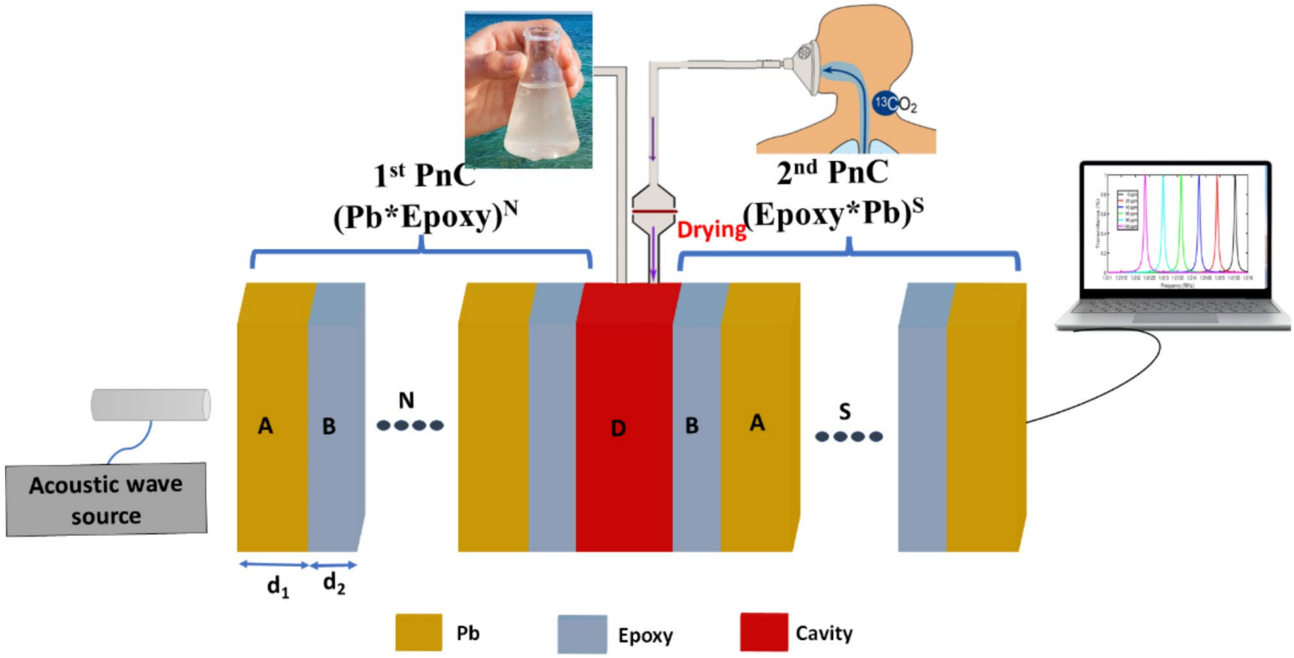

Fig. 1. 3D configuration of 1D-PnC consisting of Pb and Epoxy as $(\mathrm{PnC1})^N D\,(\mathrm{PnC2})^S$.

Material	Speed (m/s)	Density (kg/ m^3)
Pb	11,400	1960.0
Epoxy	1180	2539.5
Water	1050	1499.2
CO_2	267	1.8393
Ar	319	1.6610
O_2	326	1.3140
Air	343	1.2047
N_2	349	1.1650

Table 1. Density and speed of used materials and pure gases in human DEB[44,45]:

$$m_{22} = cos\,(k_i d_i)\,, \tag{5}$$

where the wave number $k_i = {}^{\omega}\big/_{c_i}$, the impedance $Z_i = \rho\,_i c_i$, the density $\rho\,_i$, and the longitudinal speed of sound c_i. Thus, the defect layer can be represented as[39]:

$$m_D = \begin{bmatrix} cos\,(k_D d_D) & -iZ_D sin\,(k_D d_D) \\ -i\frac{1}{Z_D} sin\,(k_D d_D) & cos\,(k_D d_D) \end{bmatrix}, \tag{6}$$

By multiplying the matrices of Pb and Epoxy layers ($m_A{*}m_b$), each unit cell can be simulated with the following matrix:

$$U_j = \begin{bmatrix} U_{11} & U_{12} \\ U_{21} & U_{22} \end{bmatrix}, \qquad j = 1,\ 2, \ldots\ \ldots\ , \tag{7}$$

where,

$$U_{11} = cos\,(k_1 d_1)\,cos\,(k_2 d_2) - \left(\frac{Z_1}{Z_2}\right) sin\,(k_1 d_1)\,sin\,(k_2 d_2)\,, \tag{8}$$

$$U_{12} = -iZ_2 cos\,(k_1 d_1)\,sin\,(k_2 d_2) - iZ_1 sin\,(k_1 d_1)\,cos\,(k_2 d_2)\,, \tag{9}$$

$$U_{21} = -i(1/Z_1) sin\,(k_1 d_1)\,cos\,(k_2 d_2) - i(1/Z_2) cos\,(k_1 d_1)\,sin\,(k_2 d_2)\,, \tag{10}$$

$$U_{22} = cos\left(k_1 d_1\right) cos\left(k_2 d_2\right) - (Z_2/Z_1) sin\left(k_1 d_1\right) sin\left(k_2 d_2\right) \quad (11)$$

To formulate the total matrix (M) of PnC1, Chebyshev polynomials will be employed to multiply the matrices of N unit cell as follows:

$$M = \begin{bmatrix} M_{11} & M_{12} \\ M_{21} & M_{22} \end{bmatrix}, \quad (12)$$

where,

$$M_{11} = U_{11}\,\beta_1 - \beta_2, \quad (13)$$

$$M_{22} = U_{22}\,\beta_1 - \beta_2, \quad (14)$$

$$M_{12} = U_{12}\,\beta_1, \quad (15)$$

$$M_{21} = U_{21}\,\beta_1, \quad (16)$$

where $\mathrm{d} = d_1 + d_2$,

$$\beta_1 = \frac{sin\left(N\Omega\, d\right)}{sin\left(\Omega\, d\right)}, \quad (17)$$

$$\beta_2 = \frac{sin\left[(N-1)\Omega\, d\right]}{sin\left(\Omega\, d\right)}, \quad (18)$$

$$\Omega = \left(\frac{1}{d}\right) acos\left[0.5\left(U_{11} + U_{22}\right)\right]. \quad (19)$$

Similarly, the total matrix ($\bar{M}$) of PnC2 can be represented. The final matrix (F) of the design can be simulated by multiplying the tree matrices $M{*}m_D{*}\,\bar{M}$, as the following:

$$F = \begin{bmatrix} F_{11} & F_{12} \\ F_{21} & F_{22} \end{bmatrix}, \quad (20)$$

where;

$$F_{11} = \left(M_{11}m_{D11} + M_{12}m_{D21}\right)\bar{M}_{11} + \left(M_{11}m_{D12} + M_{12}m_{D22}\right)\bar{M}_{21} \quad (21)$$

$$F_{21} = \left(M_{21}m_{D11} + M_{22}m_{D21}\right)\bar{M}_{11} + \left(M_{21}m_{D12} + M_{22}m_{D22}\right)\bar{M}_{21} \quad (22)$$

$$F_{12} = \left(M_{11}m_{D11} + M_{12}m_{D21}\right)\bar{M}_{12} + \left(M_{11}m_{D12} + M_{12}m_{D22}\right)\bar{M}_{22} \quad (23)$$

$$F_{22} = \left(M_{21}m_{D11} + M_{22}m_{D21}\right)\bar{M}_{12} + \left(M_{21}m_{D12} + M_{22}m_{D22}\right)\bar{M}_{22} \quad (24)$$

Finally, the transmittance (T) is:

$$T\,(\%) = 100 * \left|\frac{2Z_0}{\left(F_{11} + F_{12}Z_0\right)Z_0 + \left(F_{21} + F_{22}Z_0\right)}\right|^2 \quad (25)$$

where Z_0 denotes the impedance of the surrounding medium. The band structure of a unit cell is represented using Bloch equation as follows:

$$cos\left(Kd\right) = cos\left(k_1 d_1\right) cos\left(k_2 d_2\right) - \frac{1}{2}\left(\frac{c_1\rho_1}{c_2\rho_2} + \frac{c_2\rho_2}{c_1\rho_1}\right) sin\left(k_1 d_1\right) sin\left(k_2 d_2\right) \quad (26)$$

where K is the Bloch vector. Band structure representation will be used to determine the TMM's accuracy.Based on experimental results[26,27], the ρ and c of the aqueous solution with different NaCl concentrations (η) will be simulated as the following:

$$\rho\,\left(\frac{kg}{m^3}\right) = 0.0266277\,\eta^2 + 6.88666\,\eta + 997.261 \quad (27)$$

$$c\,\left(\frac{m}{s}\right) = 11.3527\,\eta + 1495.3 \quad (28)$$

where η is expressed in %. Depending of density on salinity in (2) is accurate for salinities from 0 to 21%[26], and (1) is a fitting to experimental data up to 26%[27], so the present study will focus only on salinities from 0 to 21%.

Figure 2 clear acoustic density of NaCl aqueous solution as a function of NaCl concentration using the proposed fitting compared with the experimental data[27] and the fitted equation[25].

The DEB of a typical person is made up of a combination of O_2 (16%), N_2 (78%), CO_2 (5%), and Ar (1%). The effective speed (c_{mix}) and density sound in the gas mixture (ρ_{mix}) at different ratios (α) is simulated as follows[40,41]:

$$c_{mix} = \frac{\sum \alpha_i \rho_i C_i}{\sum \alpha_i \rho_i}, \tag{29}$$

$$\rho_{mix} = \sum \alpha_i \rho_i, \tag{30}$$

where i is for each gas sample.

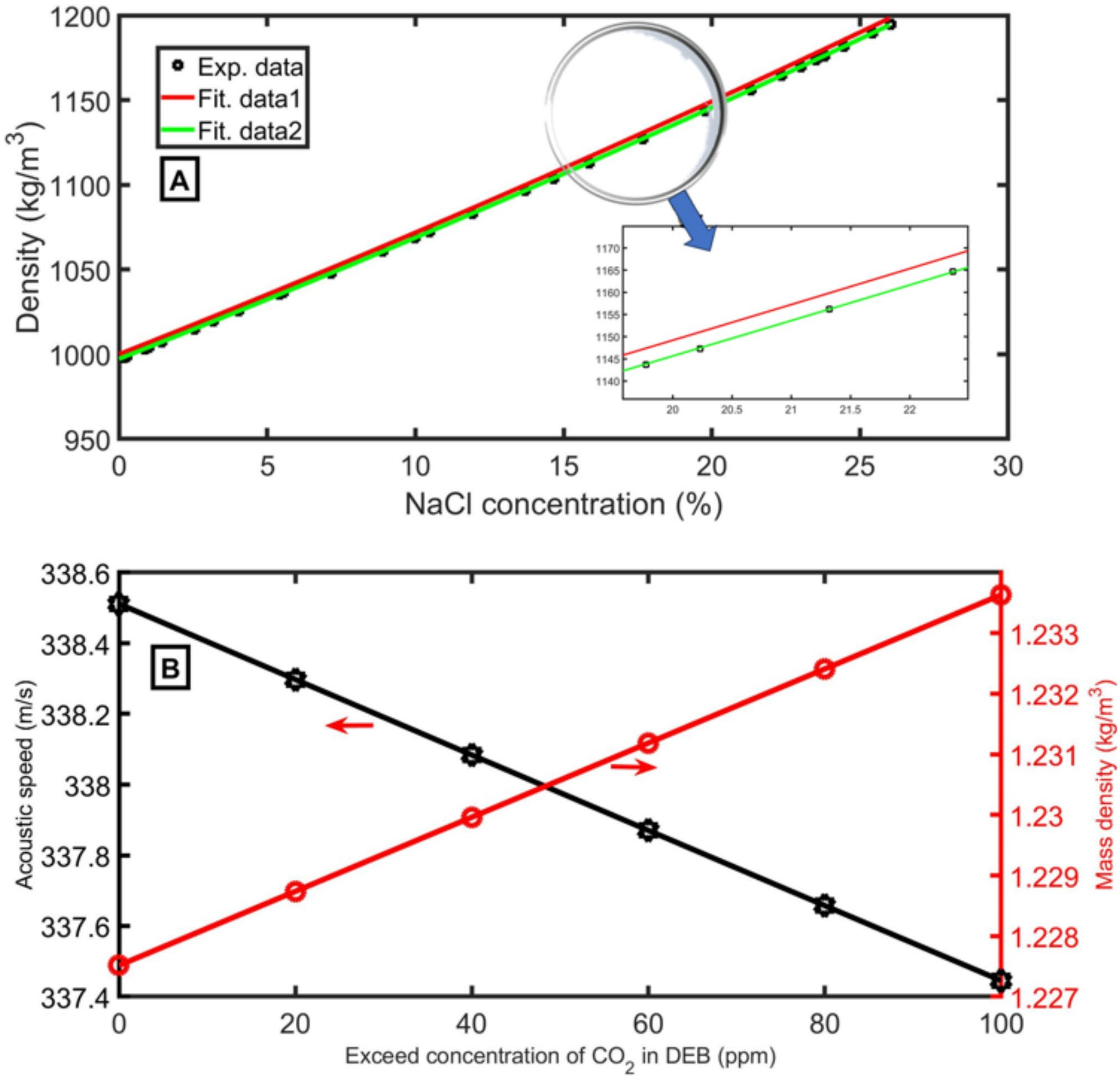

Fig. 2. (**A**) The density of NaCl aqueous solution as a function of NaCl concentration, where experimental data from Ref[27]. , Fit. data1 from Ref[25], and Fit. data2 is the present fitting, and (**B**) the speed and density of the DEB mixture at different ratios of CO_2.

Results and discussions

The physical principle of 1D-PnC sensors is based on manipulating phonon propagation through periodic variations in velocity and density. This periodic structure affects or prevents the transmittance of phonons at specific frequencies (PnBG). Creating a narrow and sensitive peak of DM using a cavity inside the structure enables the structure to behave as a sensor that detects changes in the acoustic velocity and density as a result of the concentration of the present-specific substances or biomarkers. The structure's sensitivity to any change in the analyte is influenced by the defect cavity's acoustic and geometrical properties that affect the defect mode within the PnBG. This principle has been applied in various sensor designs for detecting gases, organic materials, and biomarkers, showcasing the potential of 1D-PnCs in sensing applications.

To establish suitable (acoustic and geometrical) conditions for the proposed sensor, the parameters in Table 1 are used[42]. The thicknesses d_1, d_2 and d_D are 1.0 mm, 0.5 mm, and 0.5 mm. N and S equals 2 unitcells.

Figure 2A clear acoustic density of NaCl aqueous solution as a function of NaCl concentration using the proposed fitting compared with the experimental data in Ref[27]. and fitted equation in Ref[25]. The density and speed of sound in the mixture of DEB with exceed ratio of CO_2 is clear in Fig. 2B, according Eqs. 29 and 30.

The transmittance and band structure for both $(\mathrm{PnC1})^6$ and $(\mathrm{PnC1})^2(\mathrm{PnC2})^2$are examined, as clear in Fig. 3A,B. Both $(\mathrm{PnC1})^6$ and $(\mathrm{PnC2})^6$ creates two PnBGs in the range of concern with a nonzero localization factor. At nonzero localization factor, the acoustic wave propagation is attenuated with a coefficient of $e^{-\lambda}$. On the other hand, the incident acoustic wave propagates within the periodic configuration at zero localization factor[43], as clear in Fig. 3A. The first and second PnBGs extend from 0.345426 MHz to 0.921855 MHz and from 1.08446 MHz to 1.79438 MHz, respectively. The first and second PnBGs widths are 0.576429 MHz and 0.70992 MHz, respectively. The PnBGs are broad due to the high contrast between the acoustic responses of Pb and Epoxy. For $(\mathrm{PnC1})^2(\mathrm{PnC2})^2$, without a defect layer, a TES is excited in the second PnBG due to the localization of specific frequency (f_{TES} = 1.32433 MHz) at the interface between the two PnCs with high transmittance of 99.9% and $FWHM$ 2.91 $\times$ 10^{-4} MHz.

Salinity sensor

In Fig. 4A, the transmittance of $(\mathrm{PnC1})^2\,D\,(\mathrm{PnC2})^2$using pure water (0% NaCl). Due to the existence of D layer, a pure DM at a frequency of f_{DM} = 0.767194 MHz is excited in PnBG1. Besides, resonant peak at a frequency of $f_{DM/DM}$ = 1.36319 MHz is excited in PnBG2 due to the coupling between the TES and DM (TES/DM). These modes are due to trapping the acoustic waves in the D layer. DM and TES/DM have high transmittance (99.3% and 99.2%). As clear in Fig. 4B, by increasing the NaCl concentration from 0 to 3%, 6%, 9%, 12%, 15%, 18%, and 21%, the DM is shifted from 0.767165 MHz to 0.766163 MHz, 0.765000 MHz, 0.763689 MHz, 0.762240 MHz, 0.760665 MHz, 0.758974 MHz, and 0.757173 MHz, respectively. For TES/DM, increasing the concentration of NaCl from 0 to 3%, 6%, 9%, 12%, 15%, 18%, and 21% shifts the TES/DM from 1.36318 MHz to 1.37174 MHz, 1.38060 MHz, 1.38979 MHz, 1.39929 MHz, 1.40910 MHz, 1.41922 MHz, 1.42964 MHz, respectively. It is noted that increasing the concentration of NaCl increases the speed and density (increasing the impedance) and shifts the peak to lower frequencies when the localization factor is negative and shifts the peak to higher frequencies when the localization factor is positive, as clearly in Fig. 3A, Fig. 4B, and Fig. 5A. Figure 4B and Fig. 5A prove that the TES/DM shift is far better than the DM shift.

The term "sensitivity" (S) describes how much a sensor responds or changes its output in response to a change in the environment or amount of input. For a given change in the input quantity ($\varDelta\eta$), a highly responsive detector will create a more prominent output signal or shift ($\varDelta f_R$). In contrast, a less sensitive device would generate a less significant change or shift in the output signal. Sensitivity is a crucial feature of detection devices because it establishes their capacity to identify and quantify minute changes in the physical or chemical parameter they are intended to sense, as the following:

$$S = \frac{\varDelta f_R}{\varDelta \eta}. \tag{31}$$

FoM is used to characterize a sensor's overall efficacy. In order to distinguish between several detectors, this quantitative indicator condenses several detector attributes into a single value. Depending on the detector's type and application, the precise FoM may change. For instance, in some circumstances, the FoM could contain attributes like $FWHM$ and S. Based on their unique needs, engineers and researchers can assess and choose the best sensor for a given application with the help of the FoM that can be expressed as:

$$FoM = \frac{S}{FWHM} \tag{32}$$

The selectivity and efficiency of a detector are gauged by its Q. A greater Q means that the system has a narrower $FWHM$ and can store energy more effectively, which enables it to discern between different frequencies or signals more precisely, as follows[42,46]:

$$Q = \tfrac{f_R}{FWHM} \tag{33}$$

The smallest observable amount of input or analyte the detector can consistently quantify is the limit of detection (LoD). A lower LoD indicates a higher-sensitivity device that can pick up on minute concentrations of the desired analyte or signal.

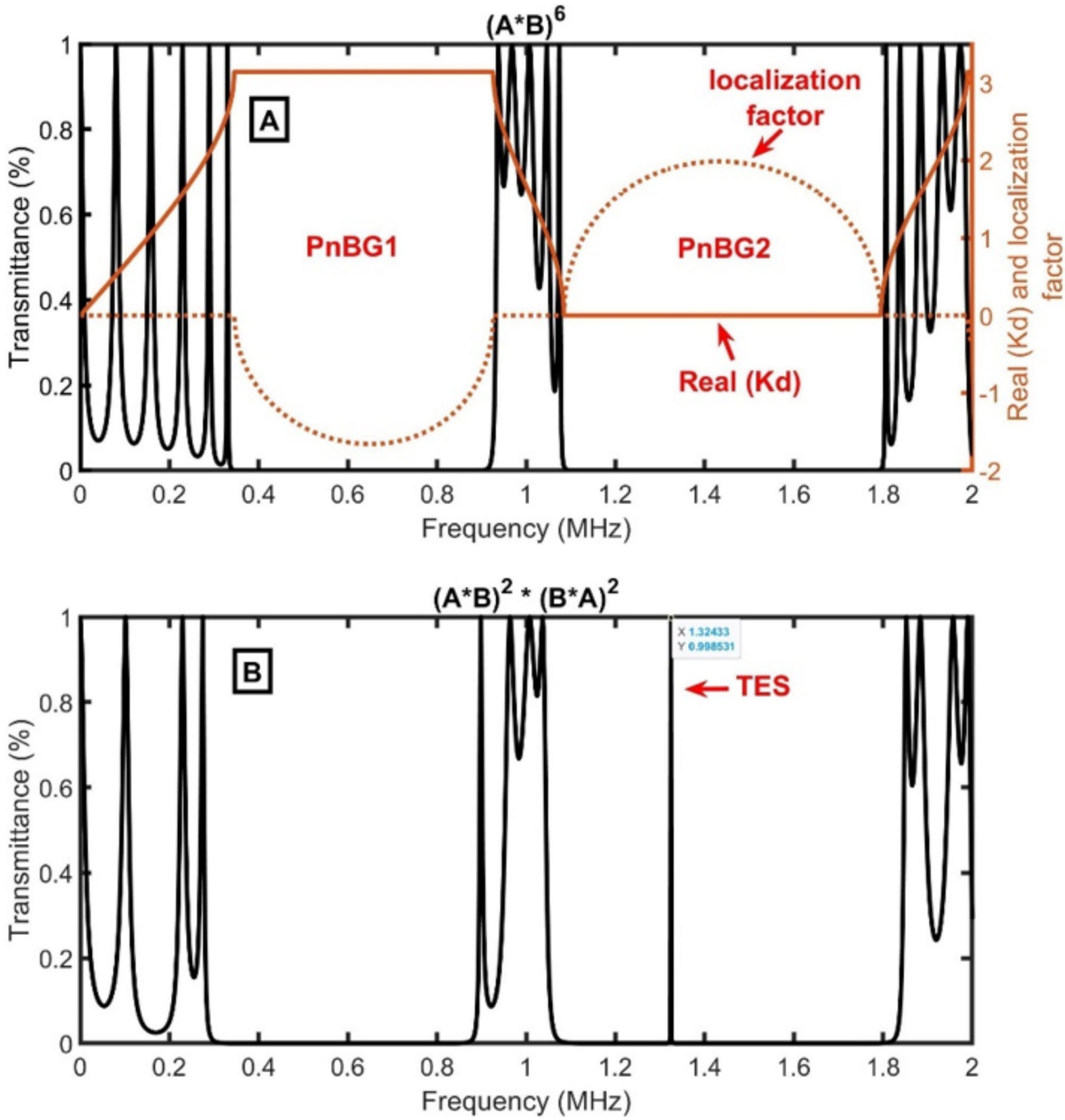

Fig. 3. (**A**) The transmittance and Bloch band structure of $(\mathrm{PnC1})^6$, and (**B**) the transmittance of $(\mathrm{PnC1})^2(\mathrm{PnC2})^2$ without any defect.

$$LoD = \frac{f_R}{20\, S\, Q}. \tag{34}$$

TES/DM has a very low $FWHM$ compared with the $FWHM$ of MD, as clear in Fig. 5B, which strongly affects the FoM, Q, and LoD of the sensor, according to Eqs. 32, 33, and 34. In Fig. 5C, the average sensitivity of TES/DM is seven times higher than the average sensitivity of MD due to the high localization in the case of coupling between TES and DM. By increasing the NaCl concentration from 3 to 21%, the sensitivity of DM in PnBG1 increases from 334 Hz/% to 600 Hz/%. For TES/DM, the sensitivity in PnBG2 increases from 2850 Hz/% to 3470 Hz/%. According to Eqs. 32, 33, FoM and Q-factor of TES/DM is very high compared with the FoM and Q of DM, as clear in Fig. 5D,E. Also, the LoD of TES/DM is very low (from 2.2×10^{-3} % to 3.2×10^{-3} %) compared with the LoD of DM, as clear in Fig. 5F. These behaviors are due to the inverse relation between

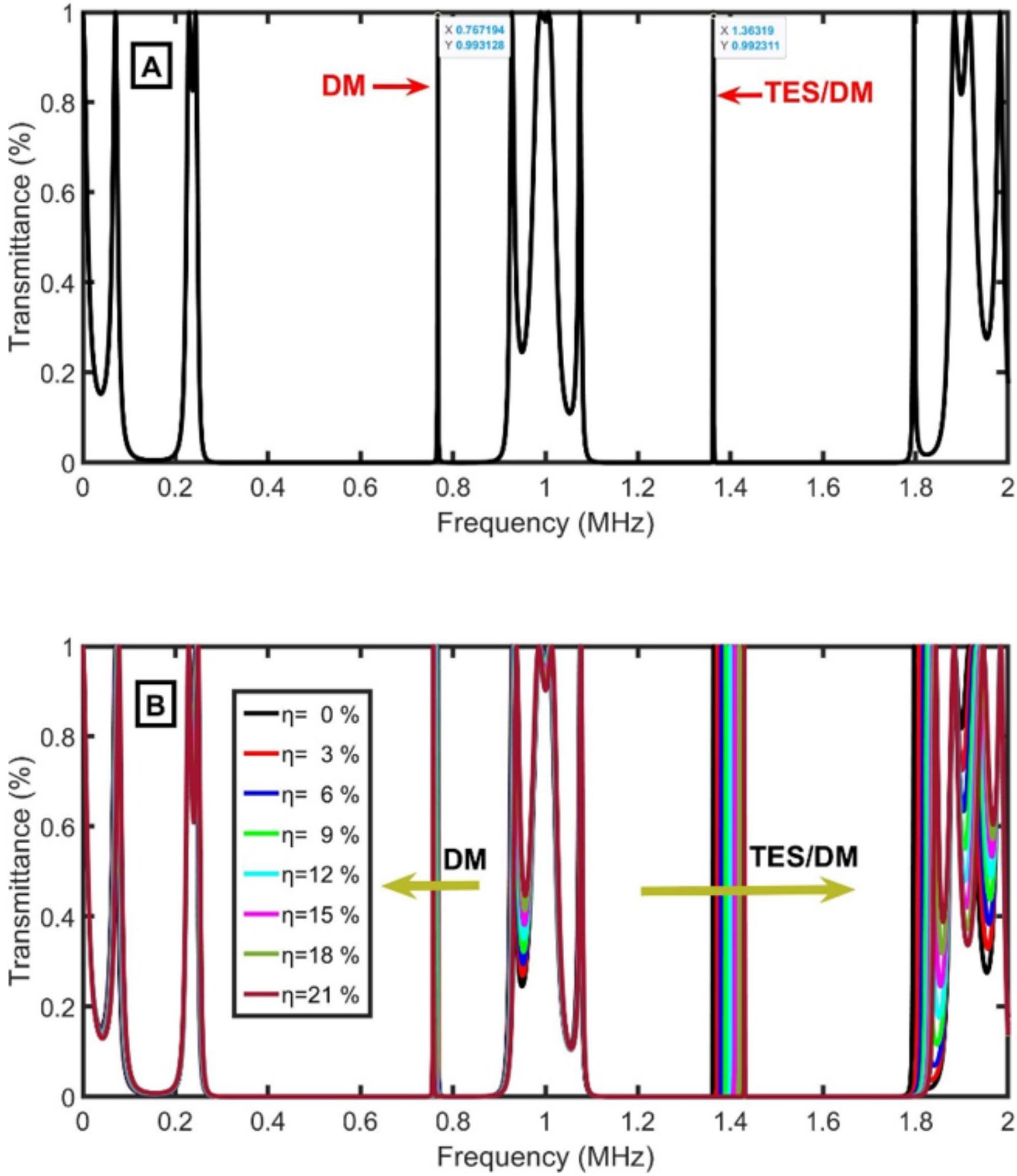

Fig. 4. The transmittance of $(\mathrm{PnC1})^2\, D\, (\mathrm{PnC2})^2$, (**A**) using pure water (0% NaCl), and (**B**) for different concentrations of NaCl.

Q and $FWHM$, the inverse relation between FoM and $FWHM$, and the direct relation between LoD and $FWHM$.

The findings suggest a hypothesis that the peak is moved to high frequencies with increasing the impedance for the positive localization factor (positive imaginary part of Bloch wavenumber) and is moved to low frequencies with increasing the impedance for the negative localization factor. For the hypothesis to be valid, it will be applied to some published studies. In Ref[29]. , Zaki et al. suggested a liquid sensor-based 1D-PnC with a negative localization factor (Fig. 6A. The peak is moved to low frequencies with increasing impedance. In Ref[47]. , Taha et

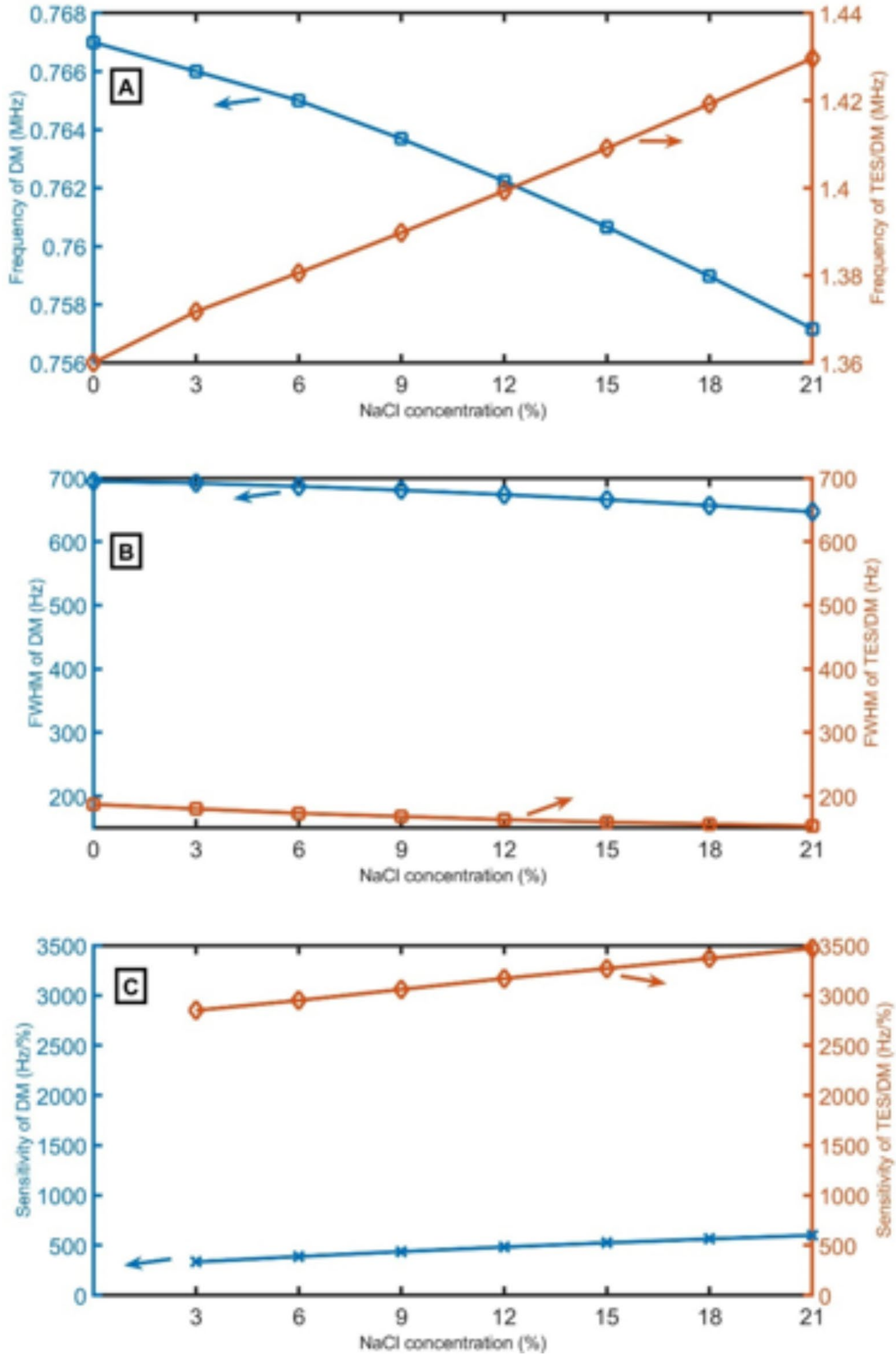

Fig. 5. (**A**) resonant frequency, (**B**) $FWHM$, (**C**) sensitivity, (**D**) FoM, (**E**) Q, and (**F**) LoD of DM and TES/DM coupling versus NaCl concentration.

al. proposed a heavy metals sensor based on 1D-PnC with a negative localization factor. The peak is moved to lower frequencies with increasing impedance. In Ref[4] , Zaky et al. designed hazardous greenhouse gases using periodic tubes as a 1D-PnC with a negative localization factor. The peak is moved to higher frequencies with decreasing impedance (Fig. 6B.

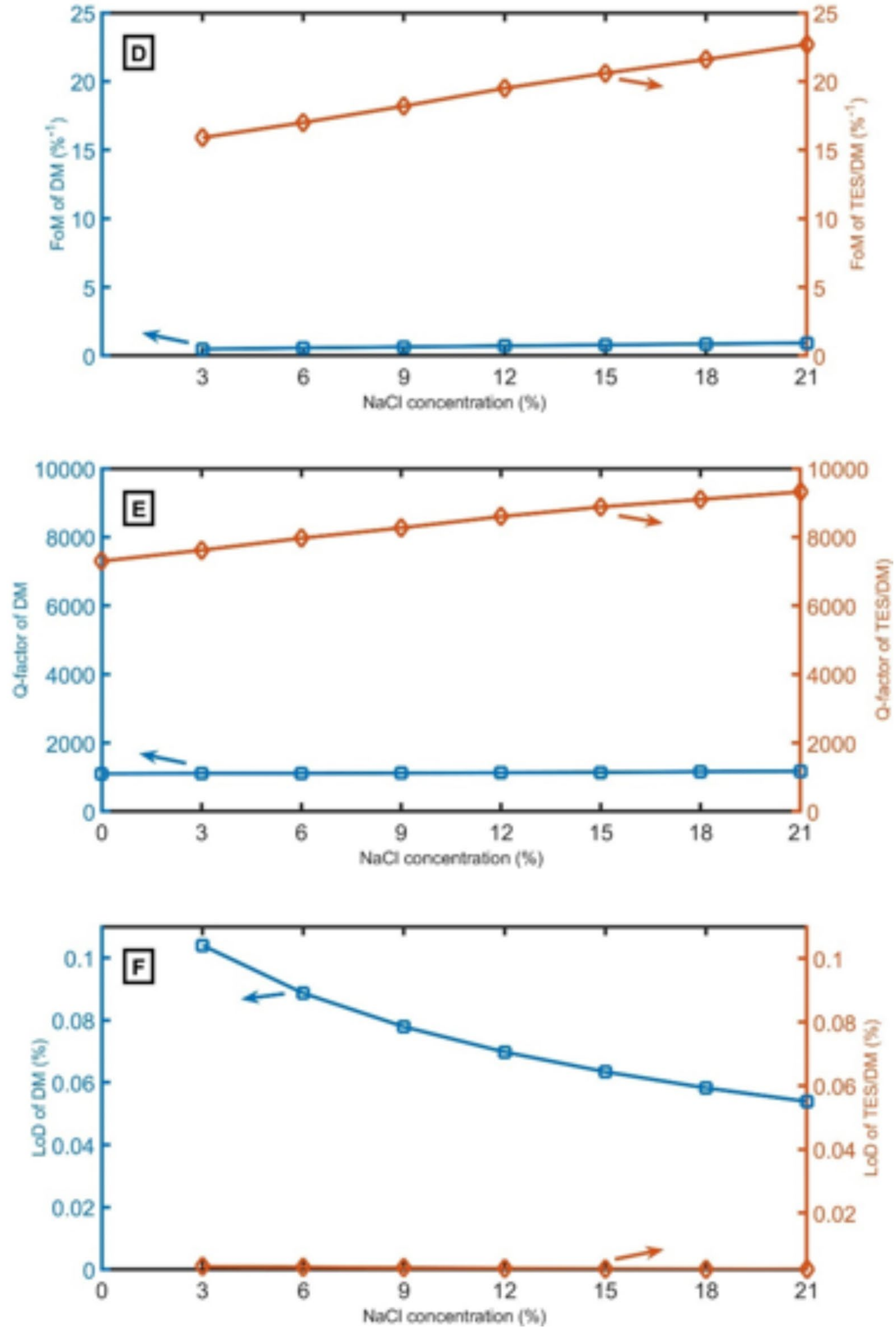

Figure 5. (continued)

Co_2 in DEB sensor

The typical DEB's density and speed are 1.2275 kg/ m^3 and 338.51 m/s, respectively, as clear in Fig. 2B. By increasing CO_2 ratio higher than the normal DEB, the speed of DEB decreases, the density increases, and the acoustic impedance slightly increases. When the DEB permeates the cavity layer, it is noticed that the TES/DM peak disappears, and the study will focus only on the DM. The localized mode is shifted from 1.01555 MHz to 1.01490 MHz, 1.01426 MHz, 1.01362 MHz, 1.01298 MHz, and 1.01245 MHz with increasing the CO_2 from 0 ppm to 20 ppm, 40 ppm, 60 ppm, 80 ppm, and 100 ppm, as clear in Fig. 7.

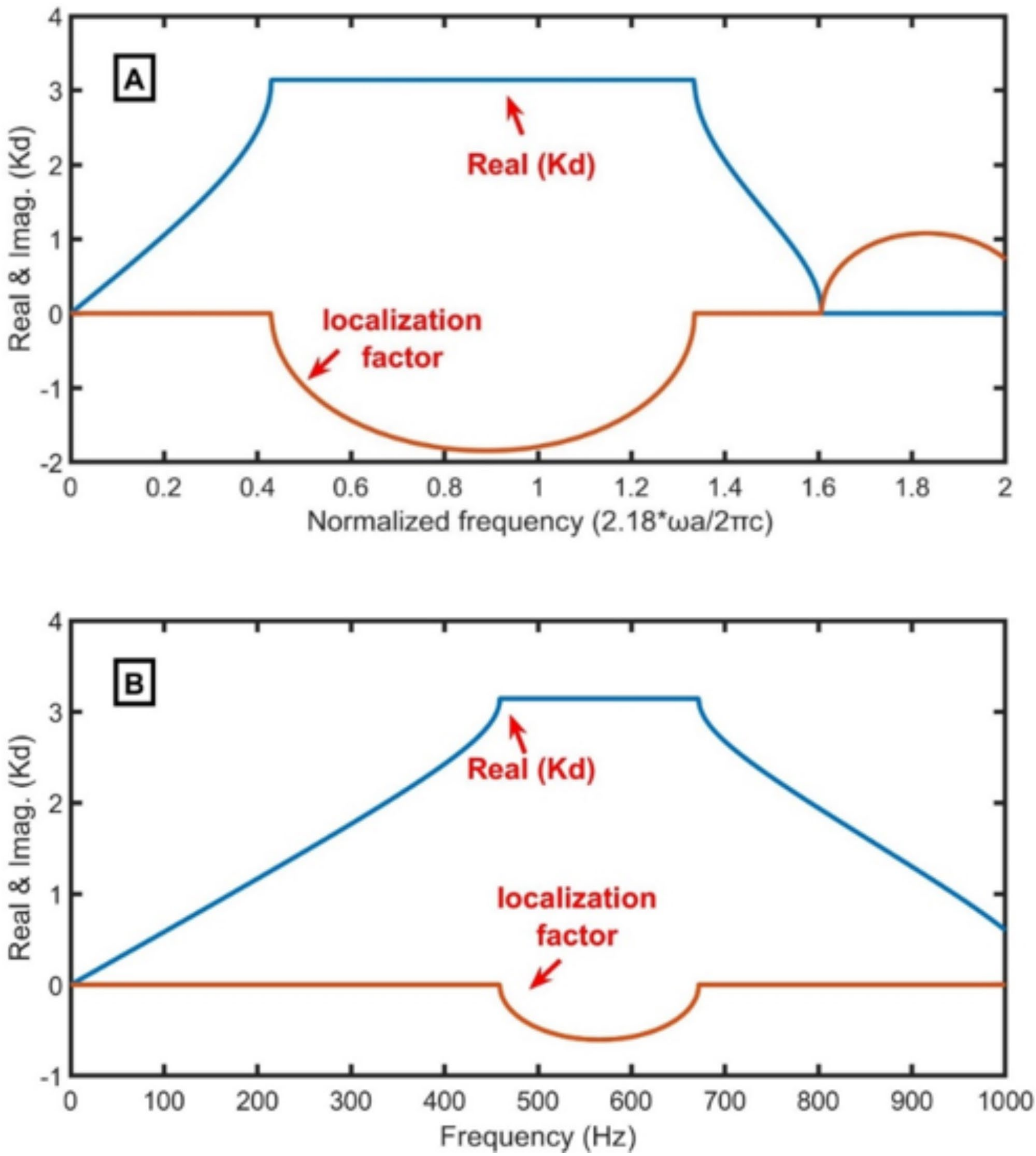

Fig. 6. The real and imaginary (localization factor) of Bloch band structure of (**A**) Pb/Epoxy unit cell in Ref[29]. , (**B**) unit cell of Ref[4].

Figure 8A clear the linearity of the proposed DEB sensor. With increasing the concentrations of CO_2 in the DEB mixture, the localized peak is moved to lower frequencies due to the increasing of the impedance of the mixture, according to Eq. 35.

$$f_R = -3.2\times\ 10^{-5}\alpha_{\ co2} + 1.01554 \tag{35}$$

$$\alpha_{\ co2} = -3.125\times\ 10^{4} f_R + 3.174\times\ 10^{4} \tag{36}$$

Using Eq. 36, the CO_2 ratio in DEB can be predicted by knowing the localized peak. The average sensitivity is 32 Hz/ppm. In Fig. 8B, FoM slightly decreases with increasing the concentrations of CO_2 in DEB mixture

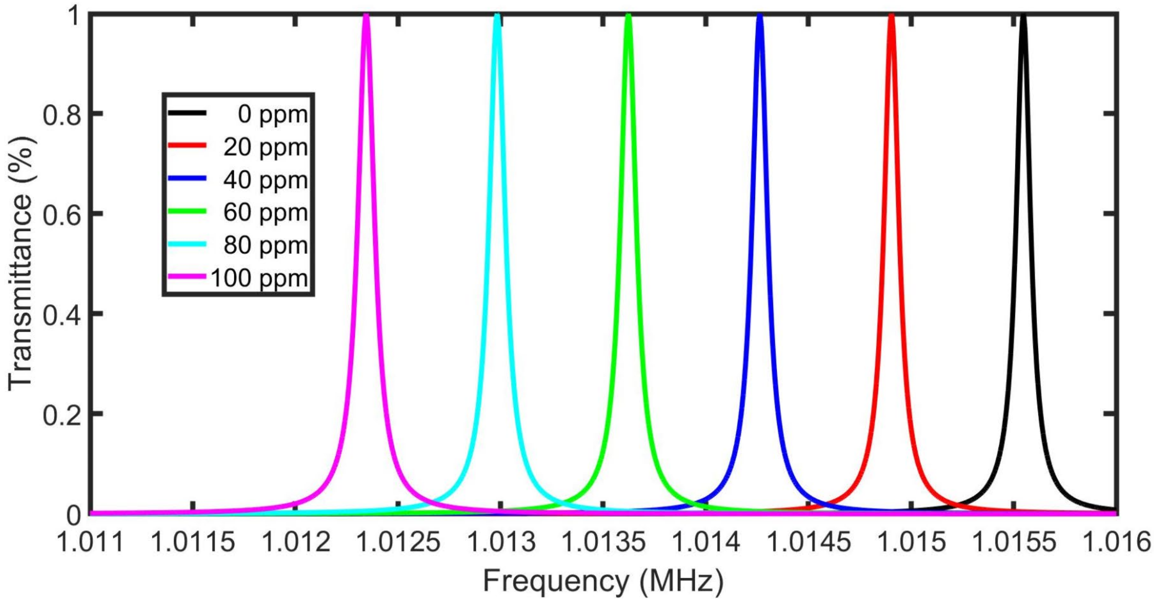

Fig. 7. The transmittance of $\left(\mathrm{PnC1}\right)^2 D\left(\mathrm{PnC2}\right)^2$ for different concentrations of CO_2 in DEB mixture.

due to the increase of $FWHM$. In Fig. 8C, the average Q and LoD are 1.12×10^4 and 0.145 ppm. To calculate the sensor resolution (RS), the following relation is used[48]:

$$RS = \frac{f_R}{Q} \tag{37}$$

The resolution of the proposed sensor changed between 84 Hz and 99 Hz for all gas samples, as clear in Fig. 8C.

In Fig. 9, different concentrations of CO_2, N_2, O_2, Ar in DEB mixture are used to check the selectivity of the proposed sensor. It is clear that the proposed sensor has high selectivity for Ar gas. Besides, it can distinguish high concentrations of CO_2. On the other hand, the results of N_2, O_2 and low concentrations of CO_2 overlab. In general, the proposed sensor can detect the changes in the DEB.

Mehaney et al.[41] discussed the use of porous silicon PnC (PSi-PnC) to detect CO_2 pollution in air. Mehaney et al. had to cap the proposed PSi-PnC with two rubber layers because the resonant mode didn't appear without these two rubber layers. Our proposed structure has been marked by the ability to excite resonant mode without adding rubber layers. In 2023, Alrowaili et al.[6] proposed 1D-PnC as a heavy metals sensor with small sensitivity and very limited FoM, as clear in Table 2. Overall, it can be concluded that the proposed structure is a unique and sensitive biosensor.

Conclusions

This study simulated symmetrical 1D-PnCs separated with a cavity to excite a topological edge state coupled with defect mode. The coupled mode recorded an average sensitivity seven times higher than the defective one, and the bandwidth of the coupled mode was four times lower than the defective one. The direction of resonant peak shift depends on the sign of the Bloch wavenumber's imaginary part (localization factor). Finally, for sensing applications, the coupled mode is advised.

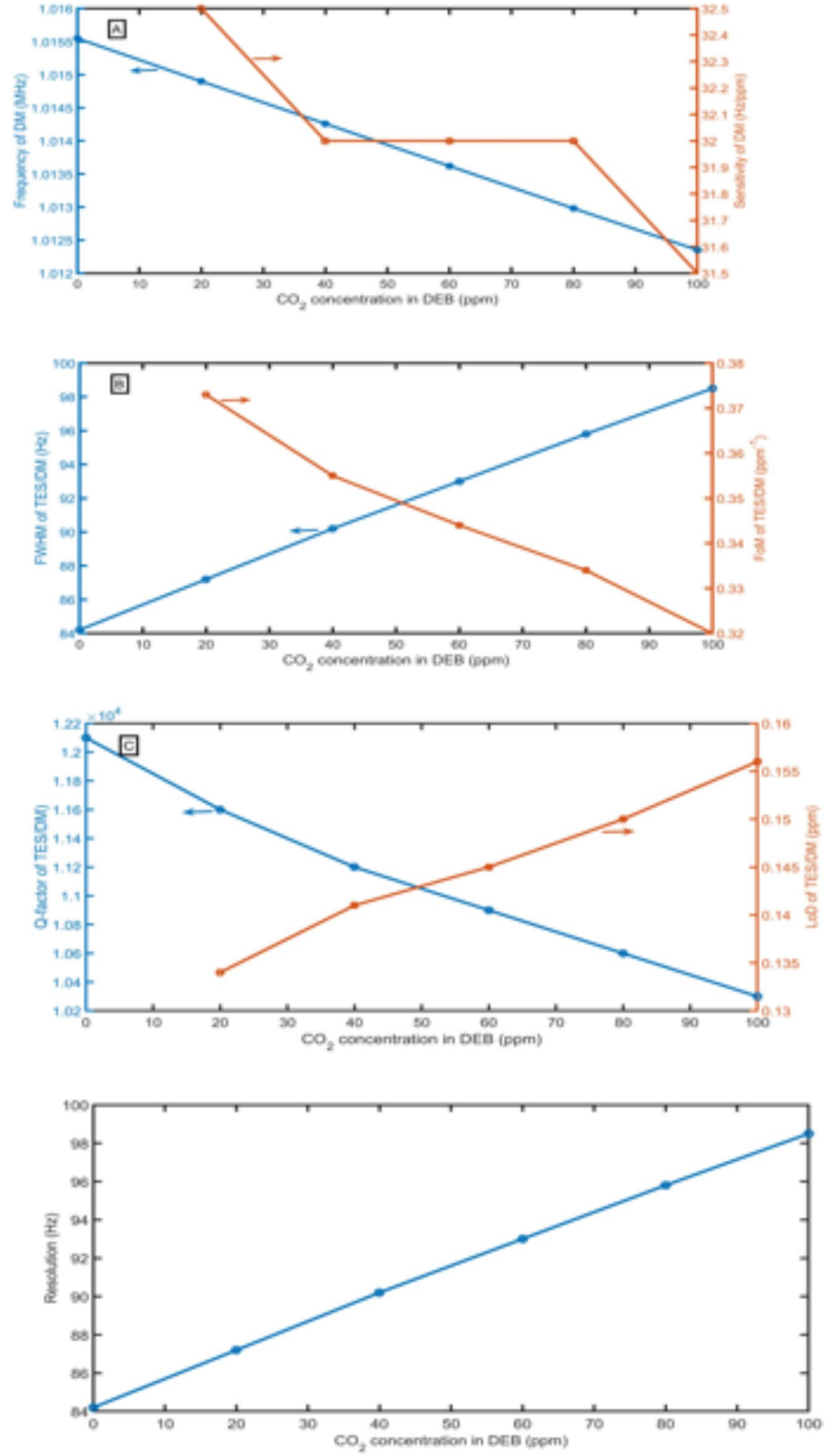

Fig. 8. (**A**) resonant frequency and sensitivity, (**B**) $FWHM\ and\ FoM$, (**C**) Q, and LoD, and (**D**) resolution of TES/DM coupling versus concentration of CO_2 in DEB mixture.

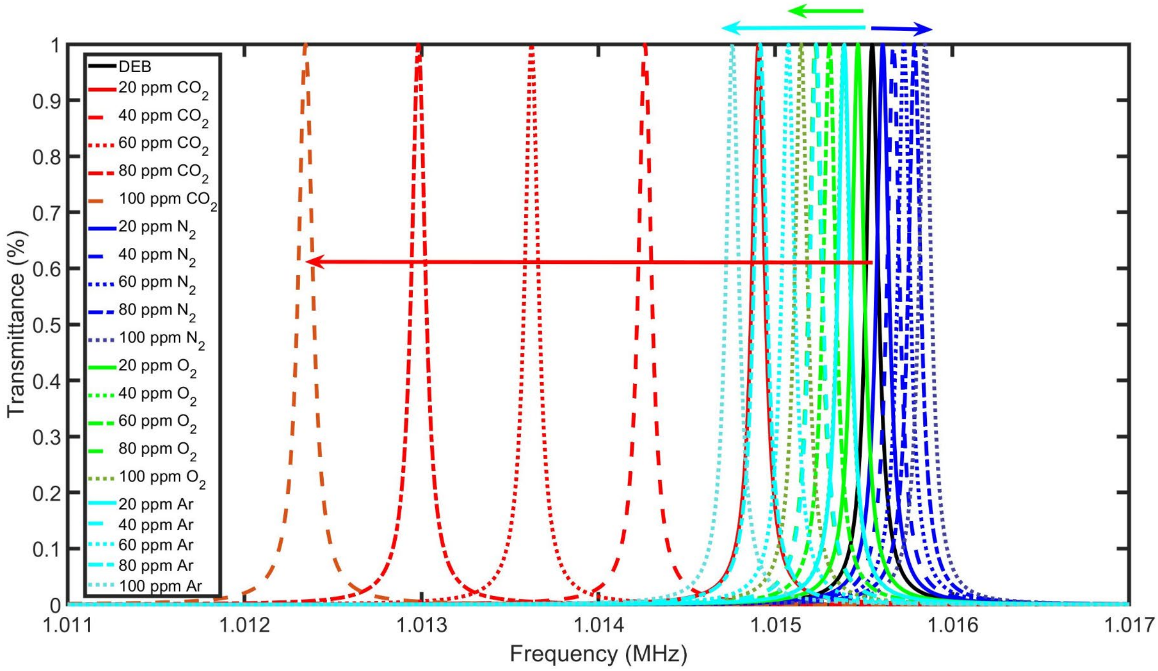

Fig. 9. The transmittance of $(\mathrm{PnC1})^2\, D\, (\mathrm{PnC2})^2$ for different concentrations of CO_2, N_2, O_2, Ar in DEB mixture.

Ref.	Sensitivity ($Hz\ ppm^{-1}$)	Type of sensor
2021[49],	0.5	Hydrocarbon vapor
2021[50],	12	Formaldehyde
2021[51],	85	Trimethylamine
2022[52],	6	Ammonia
2022[53],	0.3	Ammonia Vapor
2023[54],	0.1	Formaldehyde
2023[55],	0.1	Ammonia
Present study	32.5	CO_2 in DEB mixture

Table 2. Comparison study.

Data availability

Requests for materials should be addressed to Zaky A. Zaky.

Received: 22 May 2024; Accepted: 1 January 2025
Published online: 17 January 2025

References

1. Zaky, Z. A., Al-Dossari, M., Hendy, A. S., Badawy, W. M. & Aly, A. H. Periodic open and closed resonators as a biosensor using two computational methods. *Sci. Rep.* **14**, 11943. https://doi.org/10.1038/s41598-024-61987-3 (2024).
2. Zaky, Z. A., Al-Dossari, M., Sharma, A., Hendy, A. S. & Aly, A. H. Theoretical optimisation of a novel gas sensor using periodically closed resonators. *Sci. Rep.* **14**, 2462. https://doi.org/10.1038/s41598-024-52851-5 (2024).
3. Vasileiadis, T. et al. Progress and perspectives on phononic crystals. *J. Appl. Phys.* **129**, 160901. https://doi.org/10.1063/5.0042337 (2021).
4. Zaky, Z. A., Alamri, S., Zohny, E. I. & Aly, A. H. Simulation study of gas sensor using periodic phononic crystal tubes to detect hazardous greenhouse gases. *Sci. Rep.* **12**, 21553. https://doi.org/10.1038/s41598-022-26079-0 (2022).
5. Zaky, Z. A., Mohaseb, M., Hendy, A. S. & Aly, A. H. Design of phononic crystal using open resonators as harmful gases sensor. *Sci. Rep.* **13**, 9346. https://doi.org/10.1038/s41598-023-36216-y (2023).
6. Alrowaili, Z. et al. Heavy metals biosensor based on defective one-dimensional phononic crystals. *Ultrasonics* **130**, 106928. https://doi.org/10.1016/j.ultras.2023.106928 (2023).
7. Ameen, A. A., Al-Dossari, M., Zaky, Z. A. & Aly, A. H. Studying the effect of quantum dots and parity-time symmetry on the magnification of topological edge state peak as a pressure sensor. *Synth. Met.* **292**, 117233. https://doi.org/10.1016/j.synthmet.2022.117233 (2023).

8. Kang, Q. et al. Dual-band valley-protected topological edge states in graphene-like phononic crystals with waveguide. *Eur. Phys. J. B* **96**, 40. https://doi.org/10.1140/epjb/s10051-023-00503-4 (2023).
9. Zhang, K., Hong, F., Luo, J. & Deng, Z. Topological edge state analysis of hexagonal phononic crystals. *Acta. Mech. Sin.* **38**, 421455. https://doi.org/10.1007/s10409-021-09030-x (2022).
10. Oudich, M., Deng, Y., Tao, M. & Jing, Y. Space-time phononic crystals with anomalous topological edge states. *Phys. Rev. Res.* **1**, 033069. https://doi.org/10.1103/PhysRevResearch.1.033069 (2019).
11. Delnour, N., Bissonnette, A., Eleuch, H., MacKenzie, R. & Hilke, M. Scanning qubit probe of edge states in a topological insulator. *Phys. Lett. A* **466**, 128716. https://doi.org/10.1016/j.physleta.2023.128716 (2023).
12. Zaky, Z. A., Sharma, A., Alamri, S., Saleh, N. & Aly, A. H. Detection of fat concentration in milk using ternary photonic crystal. *Silicon* **14**, 6063–6073. https://doi.org/10.1007/s12633-021-01379-8 (2021).
13. Zhang, Z. et al. Experimental realization of multiple topological edge states in a 1D photonic lattice. *Laser Photon. Rev.* **13**, 1800202. https://doi.org/10.1002/lpor.201800202 (2019).
14. Zaky, Z. A., Mohaseb, M. & Aly, A. H. Detection of hazardous greenhouse gases and chemicals with topological edge state using periodically arranged cross-sections. *Phys. Scr.* **98**, 065002. https://doi.org/10.1088/1402-4896/accedc (2023).
15. Li, G., Wang, Y., Shi, A., Liu, Y. & Li, F. Review of seawater fiber optic salinity sensors based on the refractive index detection principle. *Sensors* **23**, 2187. https://doi.org/10.3390/s23042187 (2023).
16. Zhao, S. et al. A long period fiber grating seawater salinity sensor based on bend insensitive single mode fiber. *Opt. Fiber. Technol.* **77**, 103269. https://doi.org/10.1016/j.yofte.2023.103269 (2023).
17. Zaky, Z. A. & Aly, A. H. Highly sensitive salinity and temperature sensor using Tamm resonance. *Plasmonics* **16**, 2315–2325. https://doi.org/10.1007/s11468-021-01487-6 (2021).
18. Almawgani, A. H. et al. Photonic crystal nanostructure as a photodetector for NaCl solution monitoring: theoretical approach. *RSC Adv.* **13**, 6737–6746. https://doi.org/10.1039/D3RA00308F (2023).
19. Scheepers, M. H. et al. Diagnostic performance of electronic noses in cancer diagnoses using exhaled breath: a systematic review and meta-analysis. *Jama Netw. Open* **5**, e2219372–e2219372. https://doi.org/10.1001/jamanetworkopen.2022.19372 (2022).
20. Bhagya, D. & Suchetha, M. A capnographic sensor using acoustic virial equation for diagnostic applications. *IEEE Sens. Lett.* **4**, 1–4. https://doi.org/10.1109/LSENS.2020.3008595 (2020).
21. van Oort, P. M. et al. The potential role of exhaled breath analysis in the diagnostic process of pneumonia—a systematic review. *J. Breath Res.* **12**, 024001. https://doi.org/10.1088/1752-7163/aaa499 (2018).
22. Mazzone, P. J. Analysis of volatile organic compounds in the exhaled breath for the diagnosis of lung cancer. *J. Thorac. Oncol.* **3**, 774–780. https://doi.org/10.1097/JTO.0b013e31817c7439 (2008).
23. Zarifi, M. H. et al. Sensitivity enhancement in planar microwave active-resonator using metal organic framework for CO2 detection. *Sens. Actuators B Chem.* **255**, 1561–1568, (2018).
24. Fayaz, M. et al. Monitoring the residual capacity of activated carbon in an emission abatement system using a non-contact, high resolution microwave resonator sensor. *Sens. Actuators B* **282**, 218–224. https://doi.org/10.1016/j.snb.2018.11.038 (2019).
25. Taha, T., Elsayed, H. A. & Mehaney, A. One-dimensional symmetric phononic crystals sensor: towards salinity detection and water treatment. *Opt. Quant. Electron.* **54**, 1–16. https://doi.org/10.1007/s11082-022-03716-6 (2022).
26. Kleis, S. & Sanchez, L. Dependence of speed of sound on salinity and temperature in concentrated NaCl solutions. *Sol. Energy* **45**, 201–206. https://doi.org/10.1016/0038-092X(90)90087-S (1990).
27. Zhang & Han Viscosity and density of water + sodium chloride + potassium chloride solutions at 298.15 K. *J. Chem. Eng. Data* **41**, 516–520. https://doi.org/10.1021/je9501402 (1996).
28. Mehaney, A. & Ahmed, A. M. Modeling of phononic crystal cavity for sensing different biodiesel fuels with high sensitivity. *Mater. Chem. Phys.* **257**, 123774. https://doi.org/10.1016/j.matchemphys.2020.123774 (2021).
29. Zaki, S. E., Mehaney, A., Hassanein, H. M. & Aly, A. H. High-performance liquid sensor based one-dimensional phononic crystal with demultiplexing capability. *Mater. Today Commun.* **26**, 102045. https://doi.org/10.1016/j.mtcomm.2021.102045 (2021).
30. Liu, Z. et al. Locally resonant sonic materials. *Science* **289**, 1734–1736. https://doi.org/10.1126/Science.289.5485.1734 (2000).
31. Vasseur, J. O. et al. Experimental and theoretical evidence for the existence of absolute acoustic band gaps in two-dimensional solid phononic crystals. *Phys. Rev. Lett.* **86**, 3012. https://doi.org/10.1103/PhysRevLett.86.3012 (2001).
32. Amendola, E., Palmieri, B., Dello Iacono, S. & Martone, A. Thermally mendable self-healing epoxy coating for corrosion protection in marine environments. *Materials* **16**, 1775. https://doi.org/10.3390/ma16051775 (2023).
33. Rudawska, A. The effect of the salt water aging on the mechanical properties of epoxy adhesives compounds. *Polymers* **12**, 843. https://doi.org/10.3390/polym12040843 (2020).
34. Zaky, Z. A., Alamri, S., Zhaketov, V. & Aly, A. H. Refractive index sensor with magnified resonant signal. *Sci. Rep.* **12**, 13777. https://doi.org/10.1038/s41598-022-17676-0 (2022).
35. Zaky, Z. A., Singh, M. R. & Aly, A. H. Tamm resonance excited by different metals and graphene. *Photon. Nanostruct. Funda. Appl.* **49**, 100995. https://doi.org/10.1016/j.photonics.2022.100995 (2022).
36. Antraoui, I. & Khettabi, A. Defect modes in one-dimensional periodic closed resonators. In *International Conference on Integrated Design and Production*, 438–445. (2019).
37. Zaky, Z. A., Al-Dossari, M., Matar, Z. & Aly, A. H. Effect of geometrical and physical properties of cantor structure for gas sensing applications. *Synth. Met.* **291**, 117167. https://doi.org/10.1016/j.synthmet.2022.117167 (2022).
38. Al-Dossari, M., Zaky, Z. A., Awasthi, S. K., Amer, H. A. & Aly, A. H. Detection of glucose concentrations in urine based on coupling of Tamm–Fano resonance in photonic crystals. *Opt. Quant. Electron.* **55**, 484. https://doi.org/10.1007/s11082-023-04621-2 (2023).
39. Zaky, Z. A., Al-Dossari, M., Sharma, A. & Aly, A. H. Effective pressure sensor using the parity-time symmetric photonic crystal. *Phys. Scr.* **98**, 035522. https://doi.org/10.1088/1402-4896/acbcae (2023).
40. Hallewell, G., Crawford, G., McShurley, D., Oxoby, G. & Reif, R. A sonar-based technique for the ratiometric determination of binary gas mixtures. *Nucl. Instru. Methods Phys. Res. Sect. A Accele. Spectromet. Detect. Assoc. Equip.* **264**, 219–234. https://doi.org/10.1016/0168-9002(88)90912-6 (1988).
41. Mehaney, A. & Ahmed, A. M. Theoretical design of porous phononic crystal sensor for detecting CO2 pollutions in air. *Phys. E Low Dimension. Syst. Nanostruct.* **124**, 114353. https://doi.org/10.1016/j.physe.2020.114353 (2020).
42. Khateib, F., Mehaney, A. & Aly, A. H. Glycine sensor based on 1D defective phononic crystal structure. *Opt. Quant. Electron.* **52**, 489. https://doi.org/10.1007/s11082-020-02599-9
43. Shen, C., Kong, Y., Lu, T. J. & Yang, S. Localization of elastic waves in one-dimensional detuned phononic crystals with flexoelectric effect. *Int. J. Smart Nano Mater.* **13**, 244–262. https://doi.org/10.1080/19475411.2022.2069875 (2022).
44. Imanian, H., Noori, M. & Abbasiyan, A. Highly efficient gas sensor based on quasi-periodic phononic crystals. *Sens. Actuators B* **345**, 130418. https://doi.org/10.1016/j.snb.2021.130418 (2021).
45. Imanian, H., Noori, M. & Abbasiyan, A. A highly efficient fabry-perot based phononic gas sensor. *Ultrasonics* **124**, 106755. https://doi.org/10.1016/j.ultras.2022.106755 (2022).
46. Fang, T. Y. et al. High-performance phononic crystal sensing structure for acetone solution concentration sensing. *Sci. Rep.* **13**, 7057. https://doi.org/10.1038/s41598-023-34226-4 (2023).
47. Taha, T., Elsayed, H. A., Ahmed, A. M., Hajjiah, A. & Mehaney, A. Theoretical design of phononic crystal cavity sensor for simple and efficient detection of low concentrations of heavy metals in water. *Opt. Quant. Electron.* **54**, 625. https://doi.org/10.1007/s11082-022-04001-2 (2022).

48. Gharibi, H. & Mehaney, A. Two-dimensional phononic crystal sensor for volumetric detection of hydrogen peroxide (H2O2) in liquids. *Phys. E Low Dimension. Syst. Nanostruct.* **126**, 114429. https://doi.org/10.1016/j.physe.2020.114429 (2021).
49. Temel, F. & Ozaytekin, I. The monitoring of hydrocarbon vapor by electrospun PBINF modified QCM chemosensor. *Sens. Actuators A Phys.* **326**, 112688. https://doi.org/10.1016/j.sna.2021.112688 (2021).
50. Kang, Z., Zhang, D., Li, T., Liu, X. & Song, X. Polydopamine-modified SnO2 nanofiber composite coated QCM gas sensor for high-performance formaldehyde sensing. *Sens. Actuators B* **345**, 130299. https://doi.org/10.1016/j.snb.2021.130299 (2021).
51. Rianjanu, A. et al. Room-temperature ppb-level trimethylamine gas sensors functionalized with citric acid-doped polyvinyl acetate nanofibrous mats. *Mater. Adv.* **2**, 3705–3714. https://doi.org/10.1039/D1MA00152C (2021).
52. Zhang, D., Kang, Z., Liu, X., Guo, J. & Yang, Y. Highly sensitive ammonia sensor based on PSS doped ZIF-8-derived porous carbon/polyaniline hybrid film coated on quartz crystal microbalance. *Sens. Actuators B* **357**, 131419. https://doi.org/10.1016/j.snb.2022.131419 (2022).
53. Febrina, M., Rianjanu, A., Rajak, A., Mukti, R. R. & Djamal, M. Electrospun polyacrylonitrile nanofibers mixed with citric acid as a quartz crystal microbalance ammonia vapor sensor. *ChemistrySelect* **7**, e202103615, https://doi.org/10.1002/slct.202103615 (2022).
54. Sofa, S. A. et al. Formaldehyde gas sensors based on a quartz crystal microbalance modified with aniline-doped polyvinyl acetate nanofibers. *Analyst* https://doi.org/10.1039/D3AN01856C (2024).
55. Aflaha, R. et al. Improving ammonia sensing performance of quartz crystal microbalance (QCM) coated with nanofibers and polyaniline (PANi) overlay. *Biosens. Bioelectron. X* **13**, 100300. https://doi.org/10.1016/j.biosx.2022.100300 (2023).

Acknowledgements
The authors extend their appreciation to the Deanship of Scientific Research at King Khalid Uni-versity for funding this work through large Groups Project under grant number RGP. 2/46/45.

Author contributions
Z.A. Zaky invented the original idea of the study, implemented the computer code, performed the numerical simulations, analyzed the data, wrote and revised the main manuscript text, leader of the team. M Al-Dossari analyzed the data and discussed the results. A. S. Hendy analyzed the data and discussed the results. Y. Bouazzi analyzed the data and discussed the results. A. Boudjemline analyzed the data and discussed the results. A. H. Aly analyzed the data and discussed the results. Finally, all Authors developed the final manuscript.

Funding
The current work was assisted financially to the Dean of Science and Research at King Khalid University via the Large Group Project under grant number RGP. 2/46/45.

Declarations

Competing interests
The authors declare no competing interests.

Additional information
Correspondence and requests for materials should be addressed to Z.A.Z.